研究計画書

１．研究課題

走査型蛍光Ｘ線顕微鏡を用いた血液疾患患者血液・骨髄細胞における
細胞内元素変動解析

２．研究組織

研究代表者

病院	血液内科　５階北病棟医長	萩原將太郎

研究協力者

研究所	難治性疾患研究部長	石坂幸人
	難治性疾患研究室長	志村まり
病院	第１内科（血液内科）医長	三輪哲義

共同研究施設

所属、職名、氏名	理化学研究所播磨研究所（SPring-8）	
	X線干渉光学研究室　主任研究員	石川哲也
	大阪大学大学院工学研究科	
	精密科学専攻教授	山内和人

３．研究目的

難治性血液疾患患者の末梢血液あるいは骨髄細胞について走査型蛍光 X 線顕微鏡（SXFM；文献２）を用いて、細胞内微細構造における元素分析（エレメントアレイ解析）を行い、難治性の血液疾患患者末梢血液・骨髄細胞に特異な元素変動を見出し、疾患発症の機序解明、新たな診断および治療法の端緒を探索する。

４．研究方法

①研究対象

当センターに外来通院中あるいは入院中の血液疾患患者（急性骨髄性白血病、急性リンパ性白血病、慢性骨髄性白血病、慢性リンパ性白血病、骨髄異形成症候群、骨髄繊維症、真性多血症、再生不良性貧血、多発性骨髄腫、原発性マクログロブリン血症、発作性夜間血色素尿症）を対象とする。

②研究期間　　承認後　～　平成２２年３月

③検体の解析方法

患者末梢血と骨髄液を採取（どちらか一方でも可）。

蛍光Ｘ線専用基板に細胞を接着後固定する。
試料は理化学研究所播磨研究所 SPring-8 に搬送。
細胞の形態学的分類を施行した後、位相差型蛍光Ｘ線顕微鏡による元素分析を行う。

④目標症例数
各疾患最低３例、目標総数５０例とする。

５．患者への説明と同意

対象者には、血液疾患末梢血・骨髄細胞の特性に関する研究目的のためにサンプルを採取することを説明する。その際に、説明文書（別紙）を対象者に渡すと共にその内容を担当医が説明する。具体的には研究協力の任意性と撤回の自由、研究計画、研究目的、試料提供者にもたらされる利益および不利益、個人情報の保護、研究成果の公表、得られた医学情報の権利、費用負担に関する事項について説明する。患者（あるいは代諾者）の同意が得られた場合は同意書（別紙）に署名してもらい保存する。患者が研究目的の採取を拒否した場合はサンプルの採取は行わない。

６．個人情報の保護

当センター病院の患者検体や診療情報は、解析する前に試料の整理簿から、住所、氏名、生年月日などを削り、代わりに新しく符号をつけ、分析を行う研究者にも、患者の個人情報が漏れないようにする。解析後のサンプルは適切に処理される。

７．解析結果の開示

本研究は、血液疾患患者の協力を得て、難治性血液疾患の末梢血液細胞および骨髄細胞における疾患特有な元素変動を調べるものである。この結果、患者個人の病気の治療などに有益な結果が出る可能性は低いため原則として解析結果を本人に開示することはしない。しかし解析の結果、診療上重要な情報が見つかった場合には、診療を担当する医師から患者あるいは家族へ結果の説明を行うことがある。
研究の進み具合やその成果、学術的な意義については、定期的に、また、患者の求めに応じ、分かりやすい形で、公表あるいは説明を行う。

８．研究成果の公表

研究の成果を学会発表や学術雑誌およびデータベース上等で公表する際には、患者の個人名を匿名とし、その他のプライバシーに関することも、すべて配慮する。

９．知的財産権の扱い

患者から提供された末梢血液あるいは骨髄細胞を用いた研究によって新たな血液疾患の診断あるいは治療に役立つような情報が発見されることも考えられる。この場合、知的財産権は研究施設に帰属し、検体を提供した患者には帰属しないことを患者に説明し了解を得た後、同意書を得る。

１０．解析研究終了後の試料等の取扱の方針

解析終了後のサンプルはすべて廃棄する。

参考文献

文献 1　Fabris S, et al. Characterization of oncogene dysregulation in multiple myeloma by combined FISH and DNA microarray analysis. Genes Chromosomes Cancer 2005;42(2):117-127.

文献 2　Shimura M, et al. Element array by scanning X-ray fluorescence microscopy after cis-diamminedichloro-platinum treatment. Cancer Research 2005;65(12):4998-5002.

説明文書

研究課題名

走査型蛍光Ｘ線顕微鏡を用いた血液疾患患者血液・骨髄細胞における
細胞内元素変動解析

１．はじめに（本研究の意義及び目的）
血液疾患の多くは、その発症メカニズムが十分に解明されておらず、有用な診断法、また有効な治療法についての研究開発が必要です。本研究は、走査型蛍光Ｘ線顕微鏡(注)という新しい技術を用いて、血液細胞や骨髄細胞のミネラル（元素）変動を調べるものです。ミネラル（元素）は、細胞代謝に必須であり、バランスを損なうと体調に変化が出ることも知られています。最近、このミネラルが、腫瘍細胞などの特徴と密接に関連していることが徐々にわかってきました。この研究により、今までわからなかった血液疾患の血液細胞や骨髄細胞のミネラル変動を詳しく調べることができます。この研究により新しい診断法や治療法の開発の助けになる可能性があります。

　これからご説明することをご理解いただいた上で、この新しい技術を用いた研究のために、検査の際に末梢血液および骨髄液（どちらか一方でも結構です）を提供して頂きたく御協力をお願い致します。

（注）走査型蛍光Ｘ線顕微鏡とは？
　生体内では、適切な量の鉄、銅、カルシウム、マグネシウム、カリウム等ミネラル（元素）は代謝に必須な成分であることが知られています。この顕微鏡では、被写体（細胞）の生体内の大旨全てのミネラル（元素）を観ることができます．また、生体内では様々な細胞が存在し、それぞれ役割分担があります．近年、細胞は外界の刺激に対して、細胞のミネラル（元素）に変動を起こすことを、この顕微鏡を用いて世界で初めて観ることができるようになりました．現在、日本はこの分野において世界最高水準にあります．

２．研究協力は任意であり、撤回も自由であること
　この研究への協力への同意はあなたの自由意志で決めて下さい。また同意しなくてもそのことによって治療上何ら不利益を受けません。一旦同意した場合でも、あなたが不利益を受けることなく、いつでも同意を取り消すことができ、その場合は採取した試料（末梢血液や骨髄液）や調べた結果などは廃棄され、診療記録などもそれ以降は研究目的に用いられることはありません。

３．研究のあらまし
研究名：走査型蛍光Ｘ線顕微鏡を用いた血液疾患患者血液・骨髄細胞における元素分析
研究の目的：血液疾患患者の末梢血液および骨髄細胞について走査型蛍光 Ｘ 線顕微鏡を用

いて、細胞内の様々な元素分析を行い、血液疾患患者血液・骨髄細胞に特徴的な元素の変動を調べます。
研究機関名及び研究者・研究責任者氏名：

研究責任者

所属機関		職名	氏名
国立国際医療センター病院	血液内科	5 階北病棟医長	萩原將太郎

研究協力者

所属機関		職名	氏名
国立国際医療センター病院	血液内科	第 1 内科医長	三輪哲義
国立国際医療センター研究所	難治性疾患研究部部長		石坂幸人
	難治性疾患研究部難治性疾患研究室		志村まり

研究の方法：
血液検査の際に末梢血液約１０ｍｌおよび骨髄穿刺の検査を受ける際に余った骨髄液を約 0.5-1.0ml 程度いただきます。末梢血液か骨髄液のどちらか一方のご提供でも結構です。また、この研究のために新たに骨髄採取を行うものではありません。提供して頂いた末梢血液あるいは骨髄液中の血液細胞を分離し、位相差型蛍光 X 線顕微鏡という特殊な装置をもちいて、細胞の中に含まれる元素を測定します。
本研究の研究期間は、現在から平成２２年３月までです。
御希望があれば、この研究の計画のさらに細かい内容（研究計画書）をお渡しします。

４．予測される結果、研究協力者にもたらされる利益および不利益について
この研究は、血液疾患の患者さんの協力を得て、血液疾患の血液細胞および骨髄細胞における元素を調べるものです。研究の結果から、将来の血液疾患の患者さんにとって役に立つ情報が得られる可能性があります。しかし、あなたにとって直ちに役に立つような結果は出ないかもしれません。ただし、解析の結果、特に診療上重要と思われると判断される情報が得られることがあるかも知れません。この場合には、研究代表者より担当医師へ連絡し、担当医よりご本人へ御説明いたします。
研究から得られた解析結果につきましては、特に何かお知りになられたいことがございましたら、担当の医師を通じて研究責任者に御連絡いただければ御返事いたします。

５．個人情報が第三者から保護され、匿名化され、研究成果が公表されること
個人名につきましては当センターの個人識別情報管理者が番号で置き換えてわからないようにしてから、年齢、性別、検査所見などに関係するデータのみを添付して研究に使わせていただきます。研究の結果は、学会や学術雑誌等に発表しますが、その場合もプライバシーは保護されます。
あなたの協力によって得られた研究の成果を学会発表や学術雑誌およびデータベース上等で公表する際にはあなたの個人名を匿名とし、あなたが特定されるような状況はないように配慮されます。
本研究では、あなたの末梢血液あるいは骨髄の細胞に含まれる元素を調べますが、遺伝情報についての解析は行いません。測定後の検体（末梢血液細胞および骨髄細胞）は適切な方法（オートクレーブ＝高熱処理）により廃棄されます。
あなたの検体（末梢血液細胞および骨髄細胞）は、研究に用いられる前に氏名や診療番号などの個人情報が取り除かれ、本研究の研究代表者によって新たに番号が付されます。

これを試料の匿名化といいます。本研究ではこのように匿名化された試料を用いることで、あなたのプライバシーが保護された状態で解析を行います。また本研究計画の結果を論文として公表する際にも個人の特定化が可能になるようにはいたしません。

６．研究から生じるかもしれない知的財産権は研究協力者（あなた）には属さないこと

解析研究の結果として特許権などが生じる場合でも、残念ですが、試料を提供して下さった方のものにはなりません。あなたから提供していただいた試料を用いた研究によって、疾患の診断や治療に役立つような情報が発見され特許権などが生じることも考えられます。この様な知的所有権は研究者又は研究者の所属する施設に帰属し、試料を提供して下さったあなたには帰属しないことになります。何卒ご了解下さい。

７．研究協力は無償で行われ、研究協力者に費用の負担はないこと

検体の提供は無償でお願いいたします。もちろん研究協力者の方に費用の御負担はありません。

平成　　年　　月　　日

お問い合わせ先
国立国際医療センター血液内科　５階北病棟医長
萩原將太郎
国立国際医療センター血液内科　第１内科医長
三輪哲義
〒162-8655 東京都新宿区戸山 1-21-1
TEL 03-3202-7181（代表）
FAX 03-3207-1038（代表）

研究協力についての同意書

申請番号（　　　　　）

国立国際医療センター総長殿

私は、走査型蛍光 X 線顕微鏡を用いた血液疾患患者血液・骨髄細胞における元素分析について、下記説明者より説明文書を用いて以下の項目の説明を受けました。

・研究協力は任意であり、撤回も自由であること
・研究の意義、目的と方法
・研究から生じるかもしれない知的財産権は研究協力者に属さないこと
・研究終了後の試料等の取り扱い方法
・研究は無償に行われ、研究協力者に費用の負担はないこと

特に、以下の項目に関しては了解したことを□にチェックし、確認いたします。

□血液検査および骨髄穿刺検査の際に末梢血液および骨髄液を提供していただくこと（末梢血液あるいは骨髄液のどちらか一方でも可）
□研究協力者にもたらされる利益および不利益について
□個人情報は第三者に漏れることなく、匿名化された上で研究成果が公表されること
□末梢血液細胞および骨髄細胞の解析が終了した後は直ちに試料は廃棄されること

以上より、私は上記の研究に協力することに（下記を○で囲んで下さい）

同意します　　　　　　　　　　同意しません

平成　　年　　月　　日

研究協力者氏名（署名または記名、捺印）

説明者の職名、氏名（署名または記名、捺印）

研究成果の刊行に関する一覧表

書籍

著者氏名	論文タイトル名	書籍全体の編集者名	書　籍　名	出版社名	出版地	出版年	ページ

雑誌

発表者氏名	論文タイトル名	発表誌名	巻号	ページ	出版年
Matsuyama S, Mimura H, Yumoto, H, Sano H, Yamamura K, Yabashi M, Nishino Y, Tamasaku K, Ishikawa T, Yamauchi K,	Development of mirror manipulator for hard X-ray nanofocusing at sub-50 nm level.	Review of Scientfic Instruments	77	103102	2006
Matsuyama S, Mimura H, Yumoto, H, Hara H, Yamamura K, Sano H, Endo K, Mori Y, Yabashi M, Nishino Y, Tamasaku K, Ishikawa T, Yamauchi K,	Development of scanning X-ray fluorescence microscope with spatial resolution of 30nm using K-B mirrors optics.	Review of Scientfic Instruments	65	093107	2006

研究成果の刊行に関する一覧表

書籍

著者氏名	論文タイトル名	書籍全体の編集者名	書　籍　名	出版社名	出版地	出版年	ページ

雑誌

発表者氏名	論文タイトル名	発表誌名	巻号	ページ	出版年
Shimura,M.,Saito, A.,Ishizaka,Y	Element array by scanning X-ray fluorescence microscopy after cis-diamminedichloro-platinum (II) treatment.	Life science medical biology, Spring-8 Research frontiers 2005	2005	30-32	2006
Shimura,M., Saito, A., Matsuyama, S., Sakuma,T., Terui, Y., Ueno, K., Yumoto, H., Yamauchi, K., Yamamura, K., Mimura, H., Sano, Y., Yabashi, M., Tamasaku, K., Nishio, K., Nishino, Y., Endo,K. Hatake,K., Mori, Y., Ishizaka,Y. and Ishikawa,T.	Element array by scanning X-ray fluorescence microscopy after cis-diamminedichloro-platinum (II) treatment.	Cancer Res.	65	4998-5002	2005

研究成果の刊行に関する一覧表

書籍

著者氏名	論文タイトル名	書籍全体の編集者名	書　籍　名	出版社名	出版地	出版年	ページ

雑誌

発表者氏名	論文タイトル名	発表誌名	巻号	ページ	出版年
前島　一博	「染色体の凝縮メカニズム」	**細胞工学**	25	486-491	2006
Maeshima K, Yahata K, Sasaki Y, Nakatomi R, Tachibana T, Hashikawa T, Imamoto F, Imamoto N.	Cell cycle dependent dynamics of nuclear pores: pore-free island and lamins,	Journal of Cell Science	119	4442-4451	2006

Development of mirror manipulator for hard-x-ray nanofocusing at sub-50-nm level

S. Matsuyama, H. Mimura, H. Yumoto, and H. Hara
Department of Precision Science and Technology, Graduate School of Engineering, Osaka University, 2-1 Yamada-oka, Suita, Osaka 565-0871, Japan

K. Yamamura
Research Center for Ultra-Precision Science and Technology, Graduate School of Engineering, Osaka University, 2-1 Yamada-oka, Suita, Osaka 565-0871, Japan

Y. Sano
Department of Precision Science and Technology, Graduate School of Engineering, Osaka University, 2-1 Yamada-oka, Suita, Osaka 565-0871, Japan

K. Endo and Y. Mori
Research Center for Ultra-Precision Science and Technology, Graduate School of Engineering, Osaka University, 2-1 Yamada-oka, Suita, Osaka 565-0871, Japan

M. Yabashi
SPring-8/Japan Synchrotron Radiation Research Institute (JASRI), 1-1-1 Kouto, Mikazuki, Hyogo 679-5148, Japan

Y. Nishino, K. Tamasaku, and T. Ishikawa
SPring-8/RIKEN, 1-1-1 Kouto, Mikazuki, Hyogo 679-5148, Japan

K. Yamauchi
Department of Precision Science and Technology, Graduate School of Engineering, Osaka University, 2-1 Yamada-oka, Suita, Osaka 565-0871, Japan

(Received 26 June 2006; accepted 7 August 2006; published online 25 September 2006)

X-ray focusing using Kirkpatrick-Baez (KB) mirrors is promising owing to their capability of highly efficient and energy-tunable focusing. We report the development of a mirror manipulator which enables KB mirror alignment with a high degree of accuracy. Mirror alignment tolerances were estimated using two types of simulators. On the basis of the simulation results, the mirror manipulator was developed to achieve an optimum KB mirror setup. As a result of focusing tests at BL29XUL of SPring-8, the beam size of 48×36 nm^2 ($V \times H$) was achieved in the full width at half maximum at an x-ray energy of 15 keV. Spatial resolution tests showed that a scanning x-ray microscope equipped with the KB focusing system could resolve line-and-space patterns of 80 nm linewidth in a high visibility of 60%. © *2006 American Institute of Physics.*
[DOI: 10.1063/1.2349594]

I. INTRODUCTION

The use of x-ray microscopy using a synchrotron radiation source has expanded in the fields of medical, biological, and material sciences owing to its capability of nondestructive, high-resolution, and highly sensitivity analysis. Fresnel zone plates[1] and Kirkpatrick-Baez (KB) mirrors[2–7] are generally employed as x-ray focusing optical devices in x-ray microscopy. KB mirrors, utilizing the total reflection phenomenon, are known to be promising devices for an achromatic and highly efficient focusing system. This optical system consists of two total reflection elliptical mirrors having two focal points of a light source and a collecting point. One mirror is used for vertical focusing and the other for horizontal focusing. To realize an ideal focusing state, both nanometer-level figure accuracy on mirror surfaces and mirror alignments with a high degree of accuracy are required.[8,9]

In this study, we developed a hard-x-ray nanofocusing system using KB mirror optics for a scanning hard-x-ray microscope with a spatial resolution better than 50 nm. A paper regarding the fabrication of ultraprecise mirrors for hard-x-ray nanofocusing has already been published.[10] This article focuses on the development of a mirror manipulator to align KB mirrors accurately. Since a pair of mirrors has multiple degrees of freedom, it is difficult to adjust the alignment of the two mirrors precisely in a short time[11] without knowledge of the relationship between mirror-positioning errors and focal sizes. The required alignment accuracy for ideal focusing was investigated using both a conventional ray-tracing simulator and a wave-optical simulator.[12] The latter can simulate accurate intensity profiles under the nearly diffraction-limited condition. The mirror manipulator was compactly designed and developed on the basis of the simulation results. Using the manipulator, hard-x-ray diffraction-limited focusing with a size less than 50 nm was realized at an x-ray energy of 15 keV.

 © 2006 American Institute of Physics

Downloaded 20 Mar 2007 to 133.1.116.106. Redistribution subject to AIP license or copyright, see http://rsi.aip.org/rsi/copyright.jsp

TABLE I. Parameters of the designed elliptical mirrors.

	First Mirror	Second Mirror
Glancing angle (mrad)	3.65	4.15
Focal length (mm)	253	150
Mirror length (mm)	100	100
Length of ellipse (m)	1000.150	1000.253
Breadth of ellipse (mm)	89.406	132.019
Substrate material	Cz-(111)Si single crystal	Cz-(111)Si single crystal
Surface material	Pt	Pt
Coating thickness (nm)	50	50

II. DESIGN OF ELLIPTICAL MIRRORS

Parameters of the elliptical mirrors shown in Table I are designed to realize a focal size of less than 50 nm under the diffraction-limited condition (shown in Fig. 1). A major feature of our system is that relatively long work distances of 100 mm are selected in consideration of the practical use of an x-ray microscope system. To realize sub-50-nm focusing, these mirrors are designed to have glancing angles of approximately 4 mrad. The mirror surfaces are coated with platinum to give high reflectivity at an x-ray energy of 15 keV. In this case, the focal size was estimated using the wave-optical simulator to be 36 nm(V)×48 nm(H) for the full width at half maximum (FWHM).

III. ANGLE ERROR TOLERANCES REQUIRED FOR DIFFRACTION-LIMITED FOCUSING

We estimated the tolerance limits of mirror-positioning errors required to obtain ideal focal sizes. As is well known, glancing angle rotations, in-plane rotations, and perpendicularity between mirrors have to be finely adjusted in KB mirror alignment (shown in Fig. 2). First, the tolerance limits of these rotations were investigated using a ray-tracing simulator. The tolerances were estimated on the basis of comparison between the calculated focus size and diffraction-limited size. The obtained results are shown in Figs. 3(a)–3(c). Horizontal lines in the graphs indicate the diffraction limits predicted by the wave-optical simulator. Here, they are defined as the distance between the first minima instead of the FWHM to compare the obtained results with the diffraction limits accurately. The tolerance is defined as the range indicated by the arrows. Error tolerances required for diffraction-limited focusing are summarized in Table II.

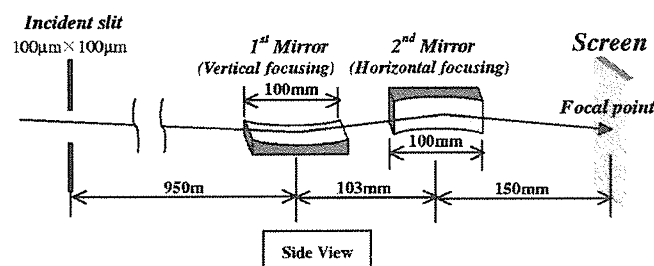

FIG. 1. Optical system using KB mirrors.

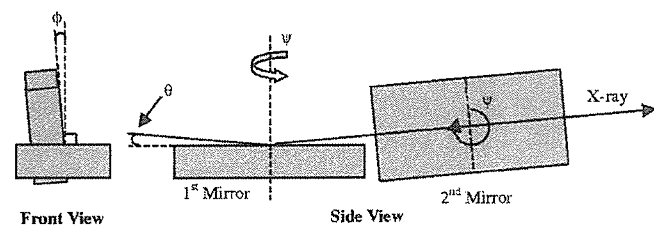

FIG. 2. Angle parameters for KB arrangement. Glancing angle rotation θ, in-plane rotation ψ, and perpendicularity φ.

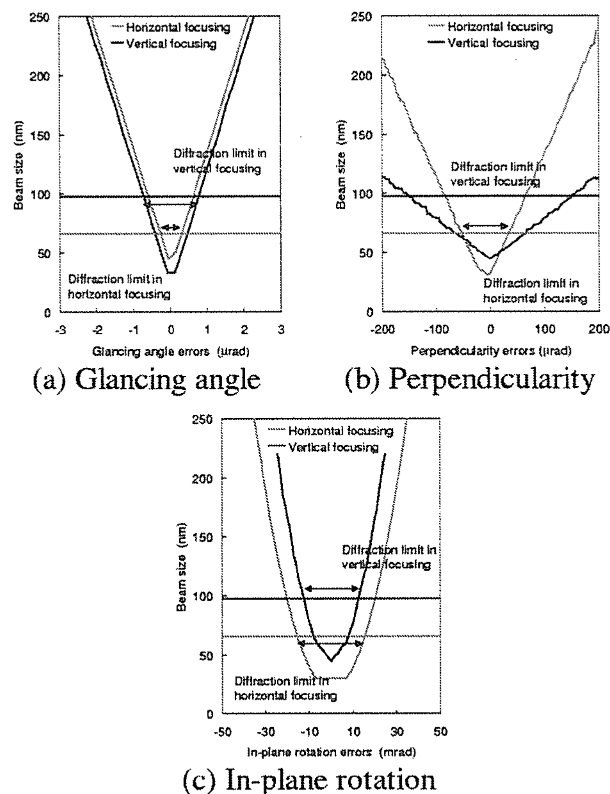

FIG. 3. Mutual relationships between angle errors and beam size calculated with ray-tracing simulator. (a) Glancing angle rotation. (b) Perpendicularity. (c) In-plane rotation. The horizontal lines indicate the diffraction limits defined as the distance between the first minima.

Since the tolerance limits of glancing angle rotations were found to be severe, they were investigated in detail using the wave-optical simulator (shown in Fig. 4). Figure 4(b) shows the relationship between glancing angle errors and FWHM. In the wave-optical simulation, the tolerance limit is defined as the angle at which the focus size increases to 120% of the smallest FWHM.

On the basis of these results, a special control system for the adjustment of glancing angles and perpendicularity between the two mirrors was designed and developed.

TABLE II. Angle error tolerances required for diffraction-limited focusing.

Alignment axis	Vertical focusing mirror	Horizontal focusing mirror
Glancing angle[a] (μrad)	±1.5	±0.9
Glancing angle[b] (μrad)	±0.6	±0.4
Perpendicularity (μrad)	±40	±40
In-plane rotation (mrad)	±13	±16

[a]Wave-optical simulator.
[b]Ray-tracing simulator.

Downloaded 20 Mar 2007 to 133.1.116.106. Redistribution subject to AIP license or copyright, see http://rsi.aip.org/rsi/copyright.jsp

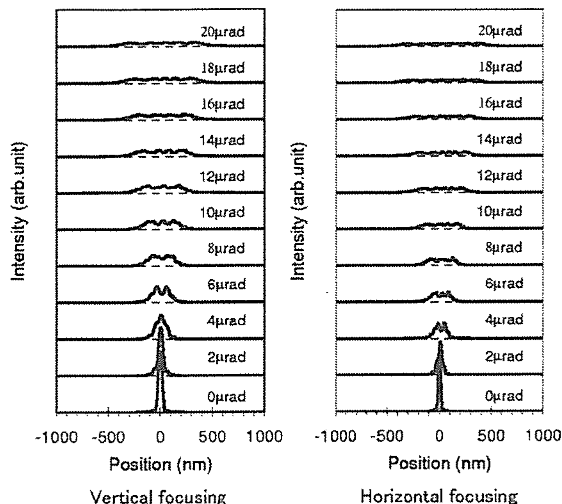

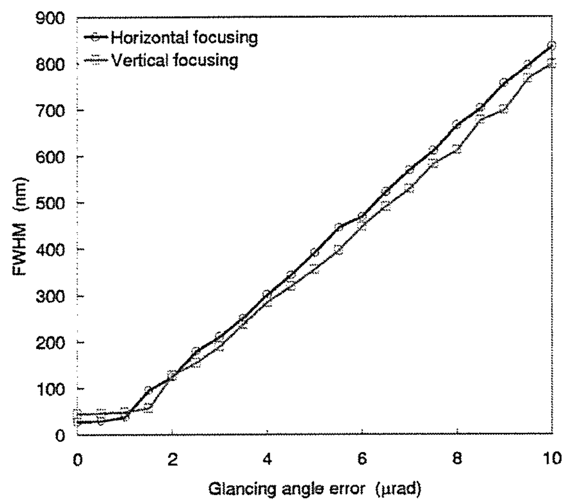

FIG. 4. Simulation results using wave-optical simulator for glancing angle alignments. (a) Series of beam profiles at every 2 μrad error from optimum glancing angle at x-ray energy of 15 keV. (b) Relationship between glancing angle errors and FWHM.

IV. DEVELOPMENT OF MIRROR MANIPULATOR

A. Adjustment system for glancing angles

A glancing angle adjustment system having a controllability of 0.04 μrad and no backlash was developed using a combined system of flexure hinges and a linear actuator (Fig. 5). In this system, the distance between the rotation center and the supporting point of the linear actuator is 100 mm; a 100 nm step of the linear actuator leads to a 1 μrad step of the glancing angle. The flexure hinges were designed to have a spring constant of 3343 N/rad to provide the linear actuator with a moderate force (approximately 3 kgf) when the glancing angle is equal to 4 mrad. Two flexure hinges were mounted on both sides of the mirrors to avoid abnormal rotation errors such as twist errors. Figure 5(b) shows the result of the performance test, in which displacement angles were measured with a microlaser interferometer (DS-80, Canon Co., Ltd.). The result shows that the system can control the

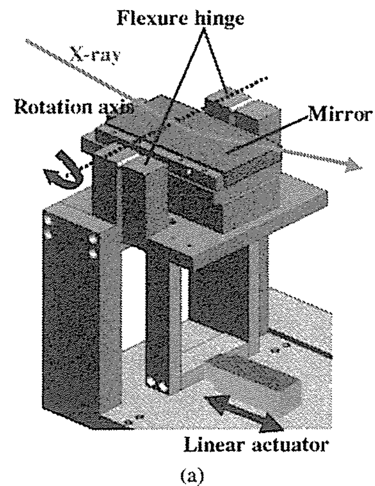

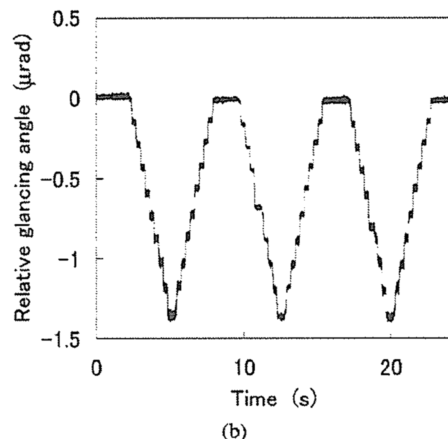

FIG. 5. (a) Adjustment system for glancing angle and (b) a result of performance test.

glancing angle without backlash over an angle range of at least 0.2 μrad.

B. Adjustment system for perpendicularity between mirrors

The perpendicularity can be preadjusted within the required accuracy because it can be determined only by the relative rollings between the two mirrors. The schematic diagram of the system is shown in Fig. 6. This system consists of two autocollimators (KT-7000, Katsura Opto Systems Co., Ltd.), a pentaprism, and tilt stages. A pentaprism, having a

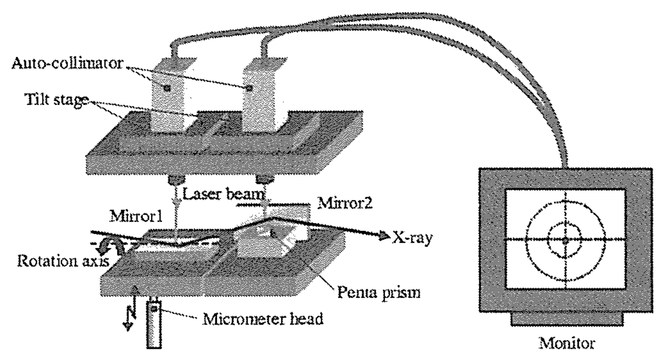

FIG. 6. Adjustment system for perpendicularity between two mirrors.

Downloaded 20 Mar 2007 to 133.1.116.106. Redistribution subject to AIP license or copyright, see http://rsi.aip.org/rsi/copyright.jsp

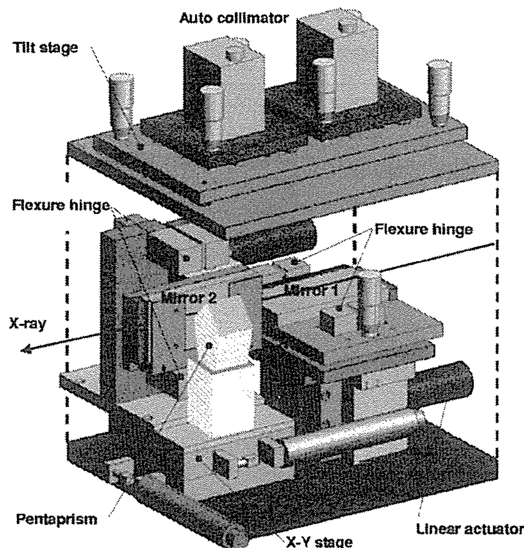

FIG. 7. Schematic diagram of developed mirror manipulator.

90° deviation tolerance of 36.4 μrad, is employed to irradiate the laser beam of the autocollimator onto the surface of the horizontal focusing mirror. The parallelism between the two autocollimators was adjusted with a sufficiently flat mirror. The most important point is that accurate perpendicularity adjustment can be achieved easily and rapidly as long as the optical axes of the two autocollimators are parallel. This system enables perpendicularity adjustment with an angle resolution of 36.4 μrad.

C. Mirror manipulator

Figure 7 shows a schematic diagram of the developed manipulator equipped with the adjustment systems. For inplane rotation adjustment, only micrometer heads are employed, because the acceptable range is more than ±10 mrad.

V. EXPERIMENTS ON FOCUSING PROPERTIES

A. Experimental setup

Focusing tests at an x-ray energy of 15 keV were performed at the 1-km-long beamline (BL29XUL) of SPring-8.[13] The mirror manipulator was placed at the third experimental hutch, which was 950 m downstream of a double crystal monochromator (shown in Fig. 8). The inplane rotations and perpendicularity were adjusted with the

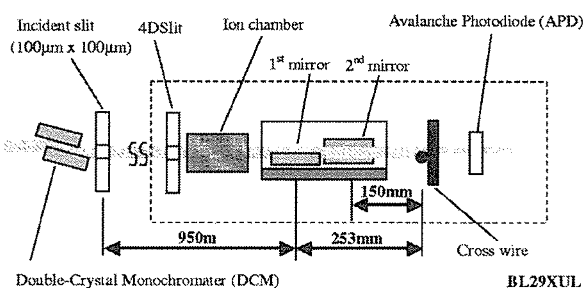

FIG. 8. Experimental setup for focusing tests.

required accuracies in advance. The glancing angle alignments were finely tuned while measuring the intensity profiles.

A wire-scanning method with a gold wire of 200 μm in diameter was employed to measure the intensity profiles at the focal plane. A linear-encoder-based feedback X-Y stage having a positioning resolution of 1 nm (Sigma Tech Co., Ltd.) was utilized to scan the wire two dimensionally.

We also demonstrated the use of a scanning x-ray microscope with a test pattern mounted on the X-Y stage close to the wire. The test pattern has periodic lines and spaces of various linewidths to investigate the best spatial resolution. In this experiment, scanning pitches are 16, 18, and 20 nm/pixel for the patterns having linewidths of 80, 90, and 100 nm, respectively. Exposure time is 1 s/pixel for each scan.

B. Experimental results

The beam intensity profiles were obtained by differentiating the curves of the intensity data measured using the wire-scanning method. As a result of focusing tests, a FWHM of 48×36 nm^2 ($V \times H$) was achieved (shown in Fig. 9). The measured profiles agree well with the wave-optically simulated profiles. This result suggests that the mirror alignments were carried out with sufficient accuracy, realizing diffraction-limited focusing.

Figure 10 shows the relationships between x-ray fluorescence intensity (tantalum $L\alpha$ line) and the beam position when the line-and-space patterns were vertically scanned with the focused beam to evaluate the spatial resolution. The peaks and valleys in the graph show tantalum lines and spaces, respectively. The subscripts in the graph correspond to the visibility between the peak and the valley. The tantalum lines of 80 nm in width were resolved with a high visibility of 60% by vertically scanning the patterns. Similarly, by horizontally scanning the patterns of 80 nm linewidth, a visibility of 55% was obtained (data not shown). The resolution evaluation with patterns of less than 80 nm linewidth was impossible, owing to the poor quality of the patterns of less than 80 nm linewidth. However, we expect that our fo-

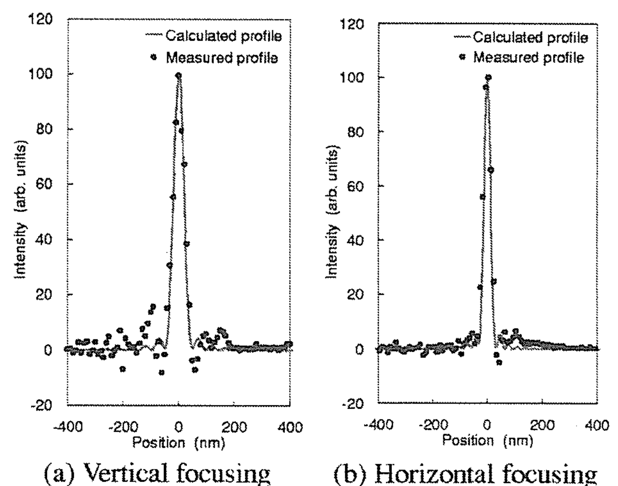

FIG. 9. Two-dimensional intensity profiles experimentally obtained, where scanning pitch is 10 nm. (a) Vertical focusing. (b) Horizontal focusing.

Downloaded 20 Mar 2007 to 133.1.116.106. Redistribution subject to AIP license or copyright, see http://rsi.aip.org/rsi/copyright.jsp

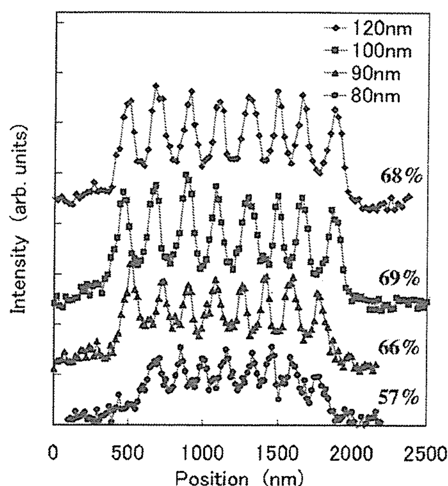

FIG. 10. Evaluation of spatial resolution in vertical direction using test patterns of various linewidths.

cusing system is capable of resolving the pattern of less than 50 nm linewidth, considering the results shown in Fig. 9. Additionally, we could not achieve better resolution in horizontal direction than that in vertical direction. The reason is that the smallest beam could not be kept for a couple of hours. If the incident angles of two mirrors changed from the best angle to have a 1.5 μrad error, the FWHM in the horizontal direction is broadened to more than 50 nm, but the FWHM in vertical direction hardly changes [see Fig. 4(b)].

ACKNOWLEDGMENTS

This research was partially supported by Grant-in-Aid for Scientific Research (S), 15106003, 2004 and 21Century COE Research, Center for Atomistic Fabrication Technology, 2004 from the Ministry of Education, Culture, Sports, Science, and Technology of Japan.

[1] Y. Suzuki, A. Takeuchi, H. Takano, and H. Talenala, Jpn. J. Appl. Phys., Part 1 **44**, 1994 (2005).
[2] P. Kirkpatrick and A. V. Baez, J. Opt. Soc. Am. **38**, 766 (1948).
[3] G. E. Ice, J.-S. Chung, J. Z. Tischler, A. Lunt, and L. Assoufid, Rev. Sci. Instrum. **71**, 2635 (2000).
[4] O. Hignette, P. Cloetens, W.-K. Lee, W. Ludwig, and G. Rostaing, J. Phys. IV **104**, 231 (2003).
[5] K. Yamauchi *et al.*, Jpn. J. Appl. Phys., Part 1 **42**, 7129 (2003).
[6] O. Hignette, P. Cloetens, G. Rostaing, P. Bernard, and C. Morawe, Rev. Sci. Instrum. **76**, 063709 (2003).
[7] W. Liu, G. E. Ice, J. Z. Tischler, A. Khounsary, C. Liu, L. Assoufid, and A. T. Macrander, Rev. Sci. Instrum. **76**, 113701 (2005).
[8] K. Yamauchi *et al.*, Rev. Sci. Instrum. **74**, 2894 (2003).
[9] H. Mimura *et al.*, Rev. Sci. Instrum. **76**, 045102 (2005).
[10] H. Mimura *et al.*, Jpn. J. Appl. Phys., Part 2 **44**, L539 (2005).
[11] S. Matsuyama *et al.*, Rev. Sci. Instrum. **76**, 083114 (2005).
[12] K. Yamauchi *et al.*, Proc. SPIE **4782**, 271 (2002).
[13] K. Tamasaku, Y. Tanaka, M. Yabashi, H. Yamazaki, N. Kawamura, M. Suzuki, and T. Ishikawa, Nucl. Instrum. Methods Phys. Res. A **686**, 467 (2001).

Downloaded 20 Mar 2007 to 133.1.116.106. Redistribution subject to AIP license or copyright, see http://rsi.aip.org/rsi/copyright.jsp

Development of scanning x-ray fluorescence microscope with spatial resolution of 30 nm using Kirkpatrick-Baez mirror optics

S. Matsuyama, H. Mimura, H. Yumoto, and Y. Sano
Department of Precision Science and Technology, Graduate School of Engineering, Osaka University, 2-1 Yamada-oka, Suita, Osaka 565-0871, Japan

K. Yamamura
Research Center for Ultra-Precision Science and Technology, Graduate School of Engineering, Osaka University, 2-1 Yamada-oka, Suita, Osaka 565-0871, Japan

M. Yabashi
SPring-8/Japan Synchrotron Radiation Research Institute (JASRI), 1-1-1 Kouto, Sayoucho, Sayogun, Hyogo 679-5148, Japan

Y. Nishino, K. Tamasaku, and T. Ishikawa
SPring-8/RIKEN, 1-1-1 Kouto, Sayoucho, Sayogun, Hyogo 679-5148, Japan

K. Yamauchi
Department of Precision Science and Technology, Graduate School of Engineering, Osaka University, 2-1 Yamada-oka, Suita, Osaka 565-0871, Japan

(Received 21 July 2006; accepted 27 August 2006; published online 11 October 2006)

We developed a high-spatial-resolution scanning x-ray fluorescence microscope (SXFM) using Kirkpatrick-Baez mirrors. As a result of two-dimensional focusing tests at BL29XUL of SPring-8, the full width at half maximum of the focused beam was achieved to be 50×30 nm^2 $(V \times H)$ under the best focusing conditions. The measured beam profiles were in good agreement with simulated results. Moreover, beam size was controllable within the wide range of 30–1400 nm by changing the virtual source size, although photon flux and size were in a trade-off relationship. To demonstrate SXFM performance, a fine test chart fabricated using focused ion beam system was observed to determine the best spatial resolution. The element distribution inside a logo mark of SPring-8 in the test chart, which has a minimum linewidth of approximately 50–60 nm, was visualized with a spatial resolution better than 30 nm using the smallest focused x-ray beam. © *2006 American Institute of Physics.* [DOI: 10.1063/1.2358699]

I. INTRODUCTION

In the hard x-ray region, x rays having beam sizes of less than 100 nm have already been realized using optical devices such as Fresnel zone plates,[1] refractive x-ray lenses,[2] and Kirkpatrick and Baez (KB) mirrors.[3–7] Hard x-ray microscopes equipped with these focusing devices are currently hot topics of research and development. Actually, the applications of x-ray microscopes have expanded to various fields of material,[8] medical and biological sciences.[9–11]

A scanning x-ray fluorescence microscope (SXFM) is an imaging tool with which the element distribution of a sample can be visualized using x-ray fluorescence generated by the focused hard x-ray irradiation of the sample. Because the excitation beam consists of hard x rays, there is no need to install samples under vacuum.

In this microscopy, spatial resolution and sensitivity depend on, respectively, beam size and photon flux. From the viewpoint of sensitivity, the combination of a synchrotron radiation source, which can generate the brightest x ray, and KB mirrors, which have high focusing efficiency, is one of the most powerful focusing systems for a SXFM. In terms of spatial resolution, the previous report[4] regarding hard x-ray nanofocusing suggests that KB mirrors enable us to obtain a nanobeam having a full width at half maximum (FWHM) of better than 40 nm. Owing to achromatic focusing using total reflection on a mirror surface, we can select the most efficient energy of x rays for various samples and experimental conditions.

In this study, we developed a SXFM which makes it possible to visualize the element distribution inside a sample at a high spatial resolution better than 30 nm using both KB mirrors focusing system and an energy-dispersive spectrometer as an x-ray fluorescence detector. The most important feature is that the mirrors employed in this study were optimally designed and fabricated to achieve diffraction-limited focusing at 45 m downstream of a virtual light source produced by a slit. Owing to the distance of 45 m, x-ray beam size is controllable over a wide range by merely adjusting a virtual light source size.

Focusing tests and demonstration of the SXFM were performed at the new second experimental hutch (EH2) of BL29XUL[12] (SPring-8). As a result of focusing tests, a beam size of 30×50 nm^2 was achieved under the diffraction-limited condition by selecting a light source size of less than 10 μm. Moreover, beam size could be controlled over a wide range from 30 to 1400 nm (at FWHM) by changing light

 © 2006 American Institute of Physics

Downloaded 20 Mar 2007 to 133.1.116.106. Redistribution subject to AIP license or copyright, see http://rsi.aip.org/rsi/copyright.jsp

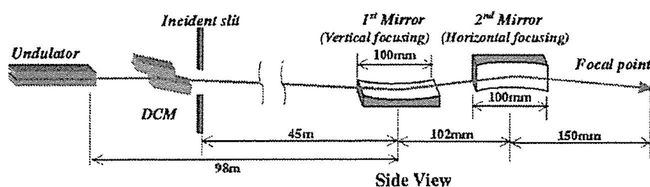

FIG. 1. Optical system designed for hard x-ray nanofocusing.

source size from 10 to 1000 μm. These results are in good agreement with simulated beam profiles. It was confirmed that the focusing system has good controllability for the SXFM. As a result of observation of a SPring-8 logo mark having a size of approximately 3×0.7 μm^2 on a test chart, the SXFM enabled us to visualize the element distribution of the logo mark at a spatial resolution better than 30 nm.

II. SCANNING X-RAY FLUORESCENCE MICROSCOPE

A. X-ray focusing optical system using KB mirrors

The new EH2 at BL29XUL of SPring-8 was newly built in May 2005 to study hard x-ray nanofocusing and hard x-ray microscopy. This hutch is placed 98 m downstream of an undulator. To utilize this hutch as efficiently as possible, KB mirrors designed specially for the hutch were fabricated with a figure accuracy of subnanometer order in Osaka University.[13–15] Available x-ray energy was selected to be less than 19 keV to be able to detect all elements using x-ray fluorescence (available within the range of 4.4–19 keV at BL29XUL). Working distance was designed to be relatively long (as long as 100 mm) considering the practical use of the x-ray microscope system, so that we keep the room where users can apply x-ray nanobeams in various experiments by only replacing a sample-scanning unit just downstream of the focusing system. A TC1 slit[16] located just downstream of a double-crystal monochromator (DCM) is used to control virtual light source size. The optical system and parameters of elliptical mirrors employed in the SXFM system are shown in Fig. 1 and Table I.

In the case of a relatively short distance of 45 m from a virtual light source to mirrors, the lower limit of beam size does not depend on only mirror aperture and focal length but also largely on light source size. However, under the condition of an adequately small source size, the smallest focus size is limited by mirror aperture size and focal length, i.e., the diffraction limit. In this case, photon flux and beam size are in a trade-off relationship. Figure 2 shows relationships between TC1 slit size and beam size predicted by wave-optical calculations. Under the conditions of a slit size of smaller than 10 μm, it is expected that diffraction-limited focusing can be realized. The slit can be no longer opened beyond a size of 1 mm because the beam broadening at the position of the slit is approximately 900×600 μm^2 (FWHM, $H\times V$). As a result of this calculation, it was expected that the beam size could be easily controlled within the range from 29 nm to micron order merely by changing the slit size from 10 to 1000 μm.

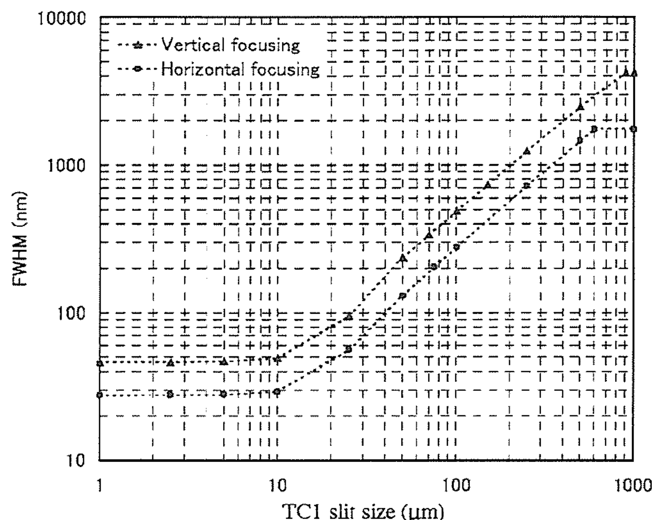

FIG. 2. Relationship between slit size and FWHMs predicated by wave-optical calculation.

TABLE I. Parameters of elliptical mirrors.

	First mirror	Second mirror
Glancing angle (mrad)[a]	3.80	3.60
Mirror length (mm)	100	100
Mirror aperture (μm)	382	365
Focal length (mm)	252	150
Numerical aperture	0.75×10^{-3}	1.20×10^{-3}
Coefficient a of elliptic function (mm)	23.876×10^3	23.825×10^3
Coefficient b of elliptic function (mm)	13.147	9.609
Diffraction limited focal size (nm, FWHM)	48	29

[a]Glancing angle at the center of the mirror.

B. SXFM system

Figure 3 shows a schematic drawing of the SXFM system. A mirror manipulator,[17] which was developed specially for high-accuracy positioning of KB mirrors, enables adjustment of mirror angle with the alignment accuracy required for diffraction-limited focusing. To detect x-ray fluorescence and transmitted x rays, respectively, a silicon drift detector (SDD, Röntec, Co., Ltd.) and a p-i-n photodiode were em-

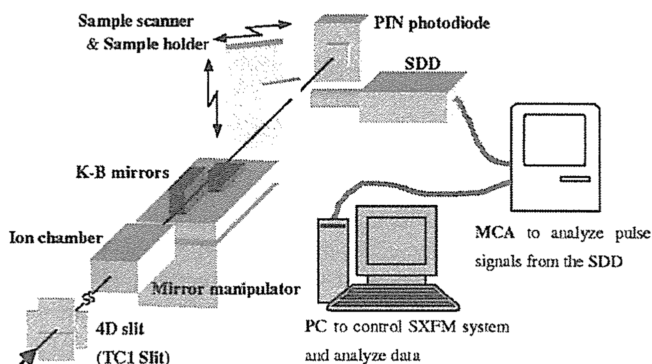

FIG. 3. Schematic drawing of scanning x-ray fluorescence microscope system.

Downloaded 20 Mar 2007 to 133.1.116.106. Redistribution subject to AIP license or copyright, see http://rsi.aip.org/rsi/copyright.jsp

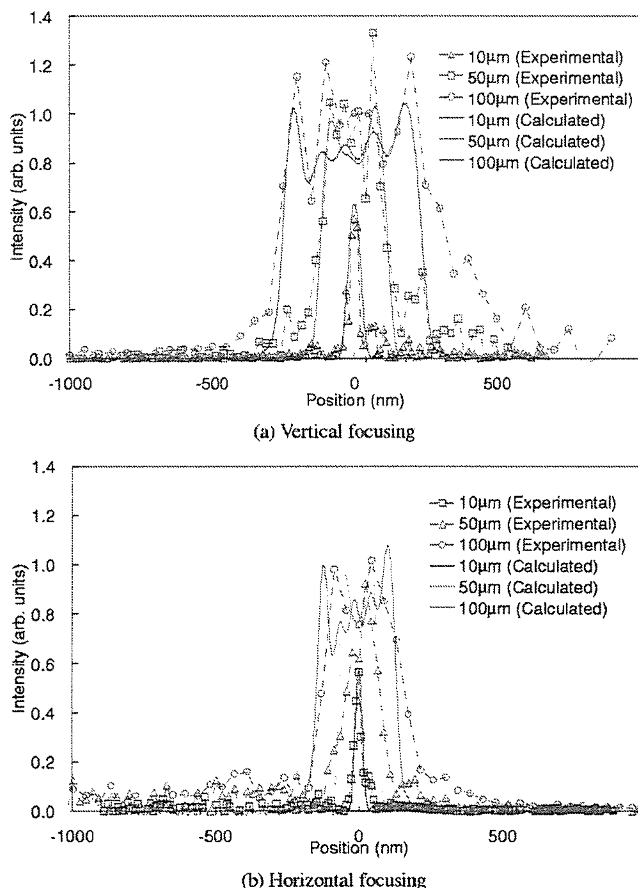

FIG. 4. Focused beam profiles obtained with KB mirrors. Subscripts at the top right show virtual source size.

ployed. An ion chamber just upstream of the mirrors is placed to normalize output data obtained with the SDD and *p-i-n* photodiode. A sample and a linear-encoder-based feedback *X-Y* stage having a positioning resolution of 1 nm (Sigma Tech, Co., Ltd.) are inclined at a 60° angle to the incident x-ray beam to set up the SDD near the sample. A cross wire is mounted on the *X-Y* stage near the sample to measure the intensity profiles at the focal plane by a wire scanning method with a gold wire of 200 μm in diameter.

III. FOCUSING TEST

Focusing tests were performed at the EH2 of BL29XUL at an x-ray energy of 15 keV. After finely tuning mirror positional alignments, beam profiles were measured by a wire scanning method, changing the virtual light source size. Experimentally obtained profiles and wave-optically simulated[18] ones are drawn, respectively, with dots and solid lines in Fig. 4. As a result of focusing tests, we could achieve two-dimensional diffraction-limited focusing having a FWHM of 30×50 nm^2 under the condition of a TC1 slit size less than 10 μm. Moreover, it was confirmed that beam size was controllable within the range of 30–1400 nm (at FWHM) by changing the slit size of a virtual source, although beam size and photon flux were in a trade-off relationship. To estimate the photon flux of focused beams, the number of x-ray photons collected by mirrors was calculated

TABLE II. Relationship between estimated beam size and measured photon fluxes.

Virtual source size ($H \times V$) (μm^2)	Beam size ($H \times V$) (nm^2)	Photon flux (photons/s)
10×10	29×48[a]	6×10^9
50×50	131×232	3×10^{11}
200×200	571×984	4×10^{12}
1000×1000 (Fully open)	$\sim 1400 \times \sim 1000$	8×10^{12}

[a]Diffraction limit.

using the value counted by the *p-i-n* photodiode. The relationship between measured photon flux and estimated beam size is summarized in Table II. As can be seen from the table, the focused beams having a photon flux from 8×10^{12} photons/s (beam size: 1400×1000 nm^2) to 6×10^9 photons/s (beam size: 30×50 nm^2) were available in the optical system.

IV. PERFORMANCE TEST FOR SXFM SYSTEM

A. Evaluation of spatial resolution

A fine test chart was observed to evaluate the zoom function and the best spatial resolution of the SXFM. The test chart (shown in Fig. 5) was microfabricated on a Si_3N_4 substrate (200 nm thickness, NTT-AT, Co., Ltd.) using a focused ion beam (FIB) system (Hitachi, Co., Ltd., FB-2100). Figure 5 shows an image of secondary electrons emitted by FIB. White and black areas correspond to tungsten (W) deposition and the substrate, respectively. In this case, the smallest logo mark has 50–60 nm linewidths.

We observed the pattern using the SXFM, gradually being magnified with the beam having a size from 500 to 30 nm. Figures 6(1)–(4) show gallium (Ga) and W distribution maps visualized using the SXFM. Map (2) corresponds to the magnified image of the area marked by a white line in map (1), and maps (3) and (4) correspond to a logo mark of SPring-8 enclosed by the dashed square in map (2). Additionally, maps (5) and (6), which were visualized at a scanning pitch of 15 nm, are magnified images of only characters in map (3) and (4). Graphs in maps (5) and (6), which are line profiles along the dashed line in the W and Ga distribution maps, are plotted with a step of 15 nm. Table III shows the scan parameters of the SXFM observations. In this test chart, gallium remains in the regions where the ion beam was irradiated because liquid gallium was employed as an

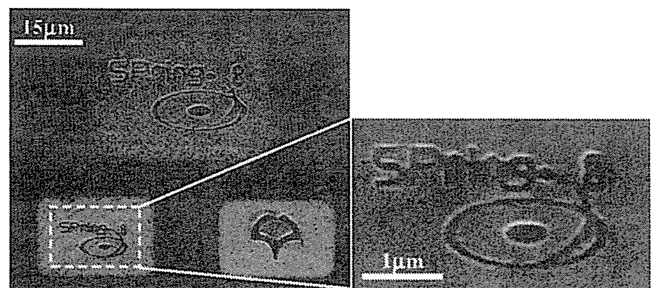

FIG. 5. Test pattern fabricated using FIB system.

Downloaded 20 Mar 2007 to 133.1.116.106. Redistribution subject to AIP license or copyright, see http://rsi.aip.org/rsi/copyright.jsp

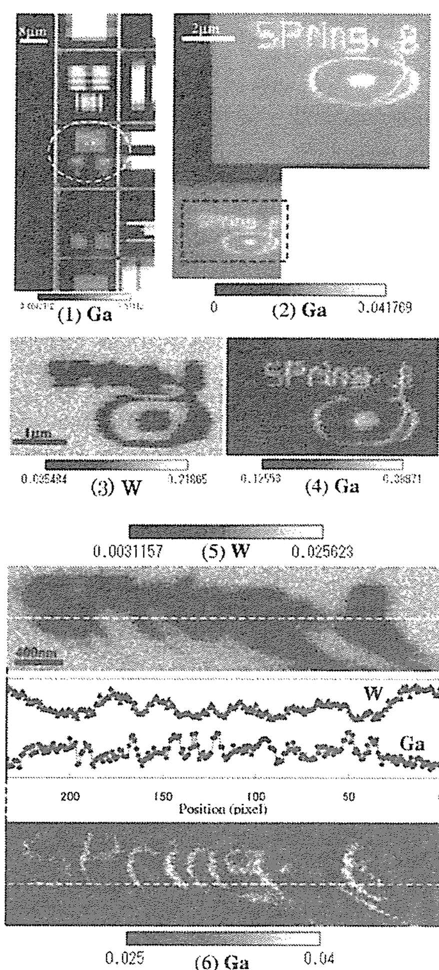

FIG. 6. Observation results of test chart using SXFM. Scan parameters are shown in Table III. Graphs of (5) and (6) show line profiles along the dash line in the W and Ga distribution maps.

ion source. As can be seen from the line profile in (6), it is found that the Ga distribution image acquired with the step of 15 nm/pixel could be visualized at a spatial resolution of 2 pixels, corresponding to 30 nm. Unlike the sharp pattern in the Ga distribution map, we cannot see sharp edges of the characters in the W distribution map in (5) because sidewall of characters patterned on the W deposition has a tapered shape. In contrast to the good results, the artifacts such as stripes and distortions are seen in Figs. 6(3)–6(6). They seem to be caused by thermal drifts of the sample, the sample scanning system, and the optical system. In this experience, the thermal stability of the whole SXFM system was within ±0.1 °C.

TABLE III. Scan parameters of SXFM. Exposure time: 1 s/pixel for each scan.

Map No.	TC1 Slit size ($V \times H$) (μm^2)	Scanning pitch (nm/pixel)	Scan area ($V \times H$) (μm^2)
(1)	150×90	1000	80×40
(2)	30×18	100	9.7×9.3
(3), (4)	10×10	30	2.25×4.02
(5), (6)	10×10	15	0.84×3.51

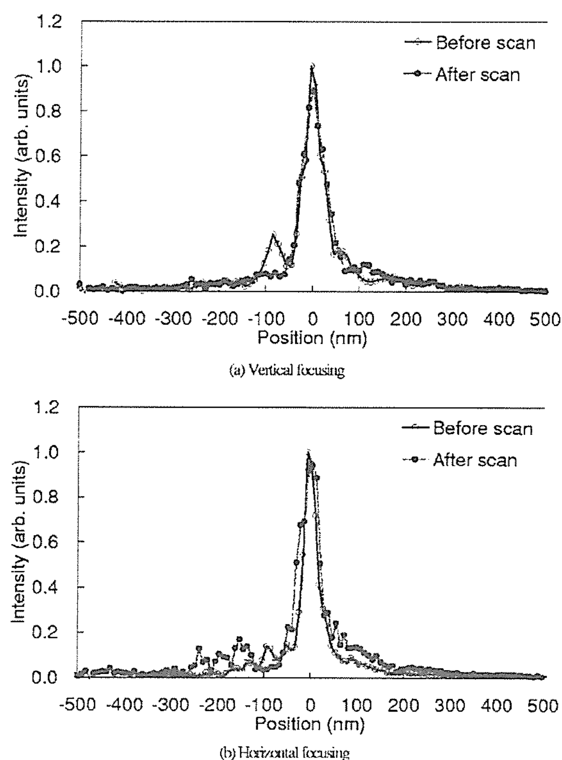

FIG. 7. Beam profiles before and after long scanning shown in Figs. 6(5) and 6(6). The time difference between the profiles is 8 h.

B. Stability of focused x-ray beam

The time required to acquire an image using a scanning x-ray microscope is 1–10 h generally, so it is important to keep the nanobeam stable during long periods of scanning. The stability of the nanobeam was evaluated by comparing beam profiles before and after high-resolution observation, as shown in Fig. 6(5) and (6) under the same condition. It took approximately 8 h to prepare the observation of the logo mark and acquire the high-resolution map. Figure 7 shows beam profiles before and after the observation. As a result of measurements of beam profiles, it was found that FWHM in horizontal focusing was broadened from 34 to 55 nm (where the beam profiles were measured at a 60° angle to the optical axis.). However, there was no change in FWHM in the vertical direction. We show results of measurements of temperature on the mirror manipulator and

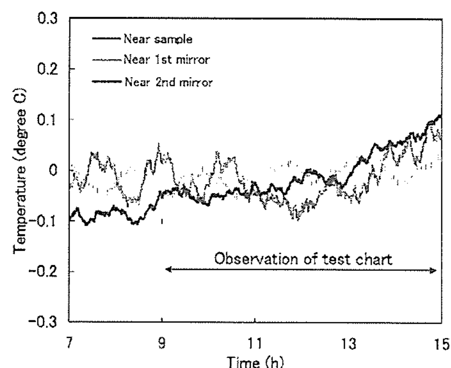

FIG. 8. Thermal stability of mirror manipulator and sample holder.

Downloaded 20 Mar 2007 to 133.1.116.106. Redistribution subject to AIP license or copyright, see http://rsi.aip.org/rsi/copyright.jsp

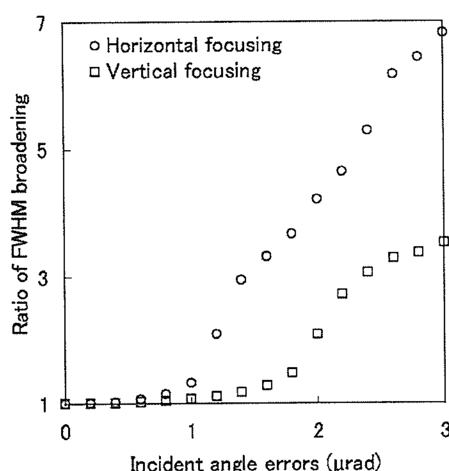

FIG. 9. Relationship between FWHM broadening and incident angle errors of the mirror. The vertical axis indicates the ratio to the best FWHM.

sample holder using thermocouples (type K) in Fig. 8. Owing to the absence of active thermal control over the whole SXFM system to avoid the vibration of the optical system, the temperature of the whole SXFM system gradually increased by 0.1–0.2 °C in 8 h. If the incident angles of two mirrors changed from the best angle to have a 1.2 μrad error in 8 h, the beam broadening caused by the misalignment is consistent with the wave-optically calculated results, showing the relationship between beam broadening and incident angle errors (shown in Fig. 9).

ACKNOWLEDGMENTS

This research was supported by Grant-in-Aid for Specially Promoted Research 18002009, 2006 and 21st Century COE Research, Center for Atomistic Fabrication Technology, 2006 from the Ministry of Education, Sports, Culture, Science, and Technology, Japan.

[1] Y. Suzuki, A. Takeuchi, H. Takano, and H. Talenala, Jpn. J. Appl. Phys., Part 1 **44**, 1994 (2005).
[2] C. G. Schroer *et al.*, Appl. Phys. Lett. **87**, 124103 (2005).
[3] P. Kirkpatrick and A. V. Baez, J. Opt. Soc. Am. **38**, 766 (1948).
[4] G. E. Ice, J.-S. Chung, J. Z. Tischler, A. Lunt, and L. Assoufid, Rev. Sci. Instrum. **71**, 2635 (2000).
[5] O. Hignette, P. Cloetens, W.-K. Lee, W. Ludwig, and G. Rostaing, J. Phys. IV **104**, 231 (2003).
[6] K. Yamauchi *et al.*, Jpn. J. Appl. Phys., Part 1 **42**, 7129 (2003).
[7] H. Mimura *et al.*, Jpn. J. Appl. Phys., Part 2 **44**, L539 (2005).
[8] T. Buonassisi, A. A. Istratov, M. A. Marcus, B. Lai, Z. Cai, S. M. Heald, and E. R. Weber, Nat. Mater. **4**, 676 (2005).
[9] K. M. Kemner *et al.*, Science **22**, 686 (2004).
[10] P. Ilinski *et al.*, Cancer Res. **63**, 1776 (2003).
[11] M. Shimura *et al.*, Cancer Res. **65**, 4998 (2005).
[12] K. Tamasaku, Y. Tanaka, M. Yabashi, H. Yamazaki, N. Kawamura, M. Suzuki, and T. Ishikawa, Nucl. Instrum. Methods Phys. Res. A **467**, 686 (2001).
[13] K. Yamauchi *et al.*, J. Synchrotron Radiat. **9**, 313 (2002).
[14] K. Yamauchi *et al.*, Rev. Sci. Instrum. **74**, 2894 (2003).
[15] H. Mimura *et al.*, Rev. Sci. Instrum. **76**, 045102 (2005).
[16] S. Goto, T. Hirono, and M. Tanaka, *MEDSI2004 Proceeding, Grenoble, France, 24–27 May 2004* (ESRF, Grenoble, 2004), p. 04-01.
[17] S. Matsuyama *et al.*, Rev. Sci. Instrum. (in press).
[18] K. Yamauchi *et al.*, Proc. SPIE **4782**, 271 (2002).

Downloaded 20 Mar 2007 to 133.1.116.106. Redistribution subject to AIP license or copyright, see http://rsi.aip.org/rsi/copyright.jsp